



1 **Debris flow modeling at Meretschibach and Bondasca catchment,**
2 **Switzerland: sensitivity testing of field data-based erosion model**

3 Florian Frank¹, Brian W. McArdell¹, Nicole Oggier², Patrick Baer³, Marc Christen⁴ and Andreas
4 Vieli³

5 ¹ Swiss Federal Institute for Forest, Snow and Landscape Research, Birmensdorf, 8903,
6 Switzerland

7 ² wasser/schnee/lawinen, Ingenieurbüro André Burkard AG, Brig-Glis, 3900, Switzerland

8 ³ Glaciology, Geomorphodynamics & Geochronology, Department of Geography, University of
9 Zurich, Zurich, 8057, Switzerland

10 ⁴ WSL Institute for Snow and Avalanche Research SLF, Davos Dorf, 7260, Switzerland

11 *Correspondence to:* Florian Frank (florian.frank@wsl.ch)

12 **Abstract**

13 Debris flow volumes can increase due to the incorporation of sediment into the flow as a
14 consequence of channel-bed erosion along the flow path. This study describes a sensitivity analysis
15 of the recently-introduced RAMMS debris flow entrainment algorithm which is intended to help
16 solve problems related to predicting the runout of debris flows. The entrainment algorithm predicts
17 the depth and rate of erosion as a function of basal shear stress based on an analysis of erosion
18 measurements at the Illgraben catchment, Switzerland (Frank et al., 2015). Starting with a
19 landslide-type initiation in the RAMMS model, the volume of entrained sediment was calculated
20 for recent well-documented debris-flow events at the Bondasca and the Meretschibach catchments,
21 Switzerland. The sensitivity to the initial landslide volume was investigated by systematically
22 varying the initial landslide volume and comparing the resulting debris-flow volume with estimates
23 from the field sites. In both cases, the friction coefficients in the RAMMS runout model were
24 calibrated using the model where the entrainment module was inactivated. The results indicate that
25 the entrainment model predicts plausible erosion volumes in comparison with field data. By
26 including bulking due to entrainment in runout models, more realistic runout patterns are predicted
27 in comparison to starting the model with the entire debris-flow volume (initial landslide plus
28 entrained sediment). In particular, lateral bank overflow – not observed during this event – is
29 prevented when using the sediment entrainment model, even in very steep ($\approx 60\text{--}65\%$) and narrow
30 (4–6 m) torrent channels. Predicted sediment entrainment volumes are sensitive to the initial
31 landslide volume, suggesting that the model may be useful for both reconstruction of historical
32 events as well as the modeling of scenarios as part of a hazard analysis.



33 1. Introduction

34 Sediment erosion caused by debris flows strongly influences the bulking behavior of debris-flows
35 (Iverson, 1997). The entrainment of sediment along the channel has been observed to considerably
36 increase the volume of debris flows at many different locations (e.g. Hungr et al., 2005; Scheuner
37 et al., 2009; Iverson et al., 2010; Berger et al., 2010a; Berger et al., 2011; Schürch et al., 2011;
38 Iverson et al., 2011, McCoy et al., 2012; Tobler et al., 2014; Frank et al., 2015). Two recent
39 extreme examples from the central Swiss Alps in the last decade showed significant bulking along
40 the flow path. In the Spreitgraben catchment (2009-2011), the overall multi-surge event volumes
41 increased to about 90'000 to 130'000 m³ – mainly due to erosion along the active channel on the
42 fan (Tobler et al., 2014; Frank et al., 2015). At the Rotlauigraben catchment (2005), about 2/3 of
43 the total volume of 550'000 m³ was eroded from the debris-flow fan during a multiple-surge
44 debris-flow event initiated by the failure of a glacier moraine during an intense rainfall event
45 (Scheuner et al., 2009). Therefore, the debris-flow erosion and bulking process should be included
46 in debris-flow runout models to increase the accuracy of runout predictions including the overall
47 runout distance, location and amplitude of lateral bank overflow but also – importantly for hazard
48 assessment – the flow and depositional pattern on the fan (Gamma, 2000; Scheuner et al., 2009;
49 Hussin et al, 2012; Han et al., 2015; Frank et al., 2015).

50 However, models which include bulking by debris flows are relatively new and their performance
51 for practical applications has not yet been systematically investigated. Most entrainment modeling
52 studies focused on the field site where the erosion data for the underlying entrainment modeling
53 concept was collected and/or exclusively dealt with a single model application field site to test their
54 concept for entrainment modeling (e.g. Han et al., 2015; Frank et al., 2015). Herein we describe the
55 systematic application of the new RAMMS entrainment/bulking model (Frank et al., 2015) for
56 several recent events in the Swiss Alps.

57 Computational debris-flow runout models, which usually neglect erosion, are often used to assess
58 runout distance and pattern (Crosta et al., 2003; D'Ambrosio et al., 2003; Medina et al., 2008;
59 Hungr and McDougall, 2009; Christen et al., 2012) and are therefore useful for hazard analysis
60 where predictions of flow intensity (e.g. the spatial distribution of flow depth and velocity) are
61 required (e.g. Scheuner et al., 2011). Because the debris flow process often was observed to cause
62 significant entrainment of sediment which can strongly influence the flow (e.g. Dietrich and
63 Dunne, 1978; Suwa and Okuda, 1980; Gallino and Pierson, 1984; Hungr et al., 1984; Benda, 1990;
64 Pierson et al., 1990; Meyer and Wells, 1997; Vallance and Scott, 1997; Berti et al., 1999; Cannon
65 and Reneau, 2000; Fannin and Wise, 2001; May, 2002; Wang et al., 2003; Revellino et al., 2004;
66 Scott et al., 2005; Godt and Coe, 2007; Breien et al., 2008; Gartner et al., 2008; Guthrie et al.,
67 2010; Procter et al., 2010; Berger et al., 2010; Berger et al., 2011; Schürch et al., 2011; Iverson et
68 al., 2011; McCoy et al., 2012; Tobler et al., 2014; Frank et al., 2015), the importance of including
69 entrainment and bulking debris flow runout modeling would be appropriate. Processed-based



70 entrainment rates using algorithms which consider the material properties of the debris flow bulk
71 (Crosta et al., 2003; D'Ambrosio et al., 2003; Medina et al., 2008; Deubelbeiss and McArdeell,
72 2012) as well as pre-specified entrainment rates which pre-define the absolute volume of eroded
73 material (Beguería et al., 2009; Hungr and McDougall, 2009; Hussin et al., 2012) have been
74 introduced in numerical runout models.

75 Recently, we introduced an erosion algorithm in the RAMMS debris flow runout model for the
76 assessment of debris flow erosion and bulking (Frank et al., 2015). The erosion algorithm uses a
77 relation between basal shear stress and erosion based on an analysis of data from the Illgraben
78 catchment, Switzerland (Frank et al., 2015; Berger et al., 2011; Schürch et al., 2011). The
79 entrainment model was used to predict the overall erosion pattern and erosion volume at the first
80 site where it was tested, the Spreitgraben, Switzerland. However, secondary erosion processes such
81 as bank collapse and small torrential flood events between the debris flow events increased the
82 uncertainty in the evaluation of the model. As a consequence, additional sensitivity tests were not
83 made. In this study we therefore focus on testing the sensitivity of the RAMMS debris flow and
84 entrainment model by assessing the sensitivity of total event volume (initial landslide volume plus
85 volume of eroded sediment) to initial flow volume. This is especially important in hazard analysis
86 where landslide scenarios are considered to trigger debris flows. For this sensitivity analysis, we
87 evaluated two Alpine catchments with diverse topography and recent well-documented debris
88 flows with volumes up to a few 10,000 m³: the Bondasca catchment in Southeastern Switzerland
89 and the Meretschibach catchment in Southern Switzerland.

90 **2. Erosion modeling study sites and available data**

91 **2.1. Meretschibach catchment, Switzerland**

92 The Meretschibach catchment is located in Southern Switzerland, adjacent to and east of the
93 Illgraben catchment (Figure 1). The catchment area is about 9.2 km² and ranges from the summit of
94 the Bella Tola mountain (3,025 m a.s.l.) to the confluence with a drainage channel (619 m a.s.l.)
95 following into the Rhone River. Debris flows in the Meretschibach currently originate mainly in
96 the Bochtür subcatchment (1.42 km² area) which is covered mostly by steep debris slopes with
97 hillslope angles on the talus deposits of up to 60%. Patches of forest are present below the treeline
98 (2,200 m a.s.l.) and at the margins of the catchment, and largely contiguous forest is found along
99 both sides of the channel below an elevation of 1,600 m. The Bochtür subcatchment is underlain by
100 Triassic sericitized quartzite and white quartzites of the Bruneggjoch formation (Gabus et al. 2008).
101 The surface has several terrace-like structures have been mapped as sacking-type features (Gabus
102 et al., 2008) and are likely sources of landslides and rockfall.

103 Sediment deposits are abundant on the steep slopes of the catchment, originating from a variety of
104 mass wasting processes. Field observations of rockfall, the presence of damaged trees, and



105 unpublished records in the community forestry archives records indicate that rockfall is a dominant
106 process for generating sediment. Observations in the source area also indicate that dry ravel of
107 gravel and sand is also common in the summer months when the hillslopes are relatively dry.
108 According to the event inventory debris flows occur mainly between April and October (Szymczak
109 et al. 2010). Small debris flows start and deposit in the upper catchment, often depositing at an area
110 of lower slope located an elevation of approximately 2,000 m a.s.l. Convective storms or long
111 duration rainfall events have been observed to mobilize these sediment deposits and initiate debris
112 flows.

113 Georadar profiles on the west side of the unforested part of the Bochtür subcatchment as well a
114 airborne georadar measurements indicate that the sediment deposits are up to 5 m thick
115 (Fankhauser et al., 2015), although independent observations of the spatial distribution of sediment
116 thickness are not available. However extrapolation of that value to other parts of the catchment
117 must be made with caution because the profiles were made on a talus deposit, which may be
118 interpreted as a depositional area on the hillslope, that exhibits little geomorphic evidence of
119 debris-flow activity.

120 In the years 2013 and 2014 several instruments and devices were installed in the catchment. In
121 October 2013, a meteorological station was installed above the initiation zone to measure
122 precipitation, temperature and snow height. Inexpensive wildlife-observation cameras recorded
123 images every 15 minutes during daylight were positioned along the most active western channel to
124 document the changes along the active channel. A debris flow monitoring station was installed on
125 23 July 2014 (Oggier et al. 2015a). It consisted of three geophones and a radar to measure the flow
126 stage. The radar is triggered by the geophones or the meteorological station and provides detailed
127 recordings of the debris flow hydrograph at a resolution of 1 Hz.

128 During summer 2014, three debris flows occurred. Because the monitoring station was installed
129 after the first event (20 July 2014), no hydrograph data are available for this event. Precipitation
130 and hydrograph data for the debris flow events on 28 and 29 July 2014 indicate that the debris flow
131 event on 28 July was triggered due to convective storms with large rainfall intensity (up to 3.3 mm
132 / 10 min) while the event 29 July 2014 initiated after a few hours of steady rainfall with moderate
133 intensity (up to 1.5 mm / 10 min). The pictures from camera 4 (see Fig. 1 for the location) clearly
134 showed that the initiation of the event on July 28 took place between 19:45 and 20:15 (UTC +2),
135 corresponding with the hydrograph measured at the observation station.

136 To obtain additional information about the initial volume and the spatial distribution of erosion, the
137 height models from 15 July and 28 October were compared. The digital elevation model of 17 July
138 was the result of a photogrammetry flight by swisstopo. The second digital elevation model (28
139 October) – which is a surface model (including vegetation) – was taken with a drone (Oggier et al.
140 2015b). The results indicate that the volume of the events eroded at the open debris slopes of



141 Bochtür was between 800 and 1,200 m³. Due to additional erosion downslope of the Bochtür
142 subcatchment, the total volume of the debris flow events was between 8,000 and 10,000 m³.

143 **2.2. Bondasca catchment, Switzerland**

144 The Bondasca catchment in south-eastern Switzerland is a tributary to the Bergell valley (Figure 2).
145 The catchment area covers about 20.9 km². The geology is dominated by the Tertiary intrusion of
146 the Bergell granite. Originating from within the North wall of Pizzo Cengalo, a rock avalanche on
147 27 December 2011 deposited about 1.5 10⁶ m³ of sediments in the upper catchment with a runout
148 of up to two kilometers from the rock wall. The deposits are up to 17 m thick and cover an area of
149 about 0.760 km² while the hydrological sub-catchment is about 1.18 km² defined by the point
150 where the channel leaves the rock avalanche deposits at the lower end of the deposit.

151 The sudden sediment input from the rock avalanche was followed by several debris flows in the
152 summer of 2012 (5 and 14 July, 25 August, 24 September) whereof the two events in July
153 evacuated about 90'000 m³ of sediments from the rock avalanche deposit. The debris flows
154 originated mainly just below a flat-shaped rock face. Some of the debris flow surges are thought to
155 have been triggered due to water accumulation at the toe of the wall causing firehose-type debris
156 flow initiation (Figure 3B and 5B) e.g. as described by Godt and Coe (2007). The slope of the
157 channel on the rock avalanche deposit varies between approx. 32° (≈ 71 %) below the flat-shaped
158 rock face and regularly decreases to 15° (≈ 33 %) at the lower end of the rock avalanche deposit.

159 **3. Debris-flow entrainment modeling**

160 The goal of this study is to evaluate the erosion algorithm implemented in the RAMMS debris flow
161 model (version 1.6.25) which has been previously described by Frank et al. (2015). In particular,
162 the sensitivity of the predicted erosion to the input parameters will be investigated, and the data sets
163 described above provide a new basis for evaluating the model. The previous study (Frank et al.,
164 2015) focused on demonstrating that more realistic runout results can be achieved when including
165 sediment entrainment and bulking into the runout model. However that study also left many
166 unanswered questions regarding the sensitivity of the model to input parameters, especially the
167 initial landslide volume, which was not possible to assess in the previous study. Herein we focus on
168 describing the sensitivity of the model to the initial landslide volume, using the two well-
169 documented events described earlier in the paper.

170 Although the RAMMS model and the erosion algorithm have been published elsewhere, they will
171 be briefly described below to provide the necessary background information for understanding the
172 model. The underlying numerical formulas of shallow water equation and the Voellmy friction
173 approach used in the RAMMS debris flow model are presented in detail in Christen et al. (2010);
174 the field-data based empirical entrainment model is described in Frank et al. (2015).



175 **3.1. Computational debris-flow model RAMMS**

176 The RAMMS debris-flow model is based on 2D depth-averaged shallow water equations for
177 granular flows in three dimensions given by the coordinates of the topographic surface of the
178 digital elevation model in a Cartesian coordinate system (x, y, z) and at time (t) (Bartelt et al.,
179 1999; Christen et al., 2010). The mass balance equation incorporates the field variables flow height
180 $H(x, y, t)$ and flow velocity $U(x, y, t)$ and is given by

$$181 \quad \dot{Q}(x, y, t) = \partial_t H + \partial_x(HU_x) + \partial_y(HU_y). \quad (1)$$

182 where $\dot{Q}(x, y, t)$ describes the mass production source term and U_x and U_y represent the depth-
183 averaged velocities in horizontal directions x and y (Christen et al., 2010). The depth-averaged
184 momentum balance equations account for the conservation of momentum in two directions x and y :

$$185 \quad S_{g_x} - S_{f_x} = \partial_t(HU_x) + \partial_x\left(c_x HU_x^2 + g_z k_{a/p} \frac{H^2}{2}\right) + \partial_y(HU_x U_y), \quad (2)$$

$$186 \quad S_{g_y} - S_{f_y} = \partial_t(HU_y) + \partial_x(HU_x U_y) + \partial_y\left(c_y HU_y^2 + g_z k_{a/p} \frac{H^2}{2}\right). \quad (3)$$

187 where the earth pressure coefficient $k_{a/p}$ is normally set to 1 when running the standard Voellmy-
188 Salm friction approach, c_x and c_y represent topographical coefficients determined from the digital
189 elevation model, S_g is the effective gravitational acceleration, and S_f the frictional deceleration in
190 directions x and y (Christen et al., 2010). The frictional deceleration S_f of the flow is determined
191 using the Voellmy friction relation (Salm et al., 1990, and Salm, 1993) and specifies the Coulomb
192 friction μ scaling with the normal stress and the turbulent friction ξ depending on the velocity
193 squared (Christen et al., 2012; Bartelt et al., 2013):

$$194 \quad S_f = \mu \cdot \rho \cdot H g \cos(\phi) + \frac{\rho g U^2}{\xi} \quad (4)$$

195 where ρ is the mass density, g is the gravitational acceleration, ϕ is the slope angle (approximately
196 similar to the internal friction angle of the material), and $H g \cos(\phi)$ is the normal stress on the
197 overflowed surface. The tangent of the effective internal friction angle of the flow material can be
198 defined for the resistance of the solid phase (the term containing μ) which extensively controls
199 deceleration behavior of a slower moving flow. On the other hand, the resistance of the viscous or
200 turbulent fluid phase (the term including ξ) prevails for a quicker moving flow (Bartelt et al.,
201 2013).



202 3.2. Debris-flow entrainment model

203 The entrainment model was constructed using field data from the Illgraben catchment in
204 Switzerland (Frank et al., 2015). The entrainment model describes the maximum erosion depth as a
205 function of channel-bed shear stress and the vertical erosion rate of channel-bed sediment erosion.
206 In detail, the model is based on the analysis of differential elevation models from pre- and post-
207 event DTMs by Schürch et al. (2011b). This provides the depth of net erosion in a cell as a function
208 of the local shear stress acting on the channel bed at the base of the flow. Similarly, the rate of
209 erosion is constrained to be at the rate reported by Berger et al., 2011, using *in situ* erosion sensors,
210 also at the Illgraben channel. In the analysis of Schürch et al (2011b), flow heights were determined
211 using values interpolated between lateral levees after each event and the shear stress τ is
212 approximated using the depth-slope product:

$$213 \quad \tau = \rho g h S \quad (5)$$

214 where ρ is the bulk mass density of the flow, h is flow height, and S is the channel slope. An
215 approximation of the typical potential erosion depth at the Illgraben follows the 50% percentile line
216 fit to the distribution of elevation change for four debris flow events (Fig. 3a in Schürch et al.,
217 2011b). The erosion algorithm implemented in the RAMMS entrainment model is defined by the
218 maximum potential erosion depth e_m and a specific erosion rate. The relationship between the shear
219 stress estimated and the measured erosion (Schürch et al., 2011b) is described as a linear function
220 of shear stress using a proportionality factor $\frac{dz}{d\tau}$ (Eq. 2). The maximum potential erosion depth e_m is
221 calculated using a critical shear stress τ_c ($= 1$ kPa) and the proportionality factor $\frac{dz}{d\tau}$ ($= 0.1$ m kPa⁻¹)
222 as a function of basal shear stress τ :

$$223 \quad e_m = \begin{cases} 0 & \text{for } \tau < \tau_c \\ \frac{dz}{d\tau} (\tau - \tau_c) & \text{for } \tau \geq \tau_c \end{cases} \quad (6)$$

224 The average rate of erosion recorded at the erosion sensor site during the Illgraben debris flow
225 event of 1 July 2008 (Berger et al., 2011) is used to define a specific erosion rate $\frac{dz}{dt}$.

$$226 \quad \frac{dz}{dt} = -0.025 \text{ for } e_t \leq e_m \quad (7)$$

227 When the critical shear stress τ_c is exceeded, sediment can be entrained from the channel.
228 Entrainment stops when the actual erosion depth e_t reaches the maximum potential erosion depth
229 e_m (Eq. 2). Normally, the specific erosion rate is implemented using the default value $\frac{dz}{dt} =$
230 -0.025 ms⁻¹ (Eq. 3) as presented in Frank et al. (2015). However, the model also allows to



231 account for larger or smaller erosion scenarios by either doubling the rate or cutting it in half. In
232 this study, we will use these variable erosion rates for testing the sensitivity of the model.

233 **3.3. Erosion model setup**

234 **3.3.1. Topographic resolution**

235 This study focuses on the evaluation of the sensitivity of the predicted (modeled) channel-bed
236 erosion in relation to the initial volume (e.g. initial landslide size) and the comparison of the model
237 results and the erosion pattern observed in the field. The ability to reproduce the observed erosion
238 patterns highly depends on a realistic representation of the channel morphology where the channel
239 is clearly visible in the DTM (Deubelbeiss et al., 2010 and 2011; Scheuner et al., 2011; Hohermuth
240 and Graf, 2014) and the channel dimensions (e.g. cross-sectional area) in the DTM have to be
241 similar to what is observed in the field (e.g. Frank et al., 2015). In this study, the initial topographic
242 data available for the Meretschibach catchment (described above) are on a square grid of 0.5 m for
243 a channel with a width of 2 to 4 m. At the Bondasca catchment data are available on a 2 m square
244 grid for channel varying in width from about 5 to 20 m. Although a channel width to DTM grid
245 spacing ratio of more than 5 to 10 would probably produce more accurate results, such data are
246 generally unavailable and the increase in the time for a simulation would be impractical.

247 **3.3.2. Erosion model starting condition: block release and input hydrograph**

248 The type of initial release mechanism, lock release or input hydrograph, can be determined based
249 on field observations, potential model constraints and previous modeling experience using the
250 RAMMS debris flow model (Bartelt et al., 2013). Recent debris flow modeling studies
251 (Deubelbeiss et al., 2010; Deubelbeiss et al., 2011; Han et al., 2015) summarized that debris flows
252 in steep channels are mostly triggered by the sudden destabilization of material originating from
253 lateral bank collapses or dam-type deposits located within the channel itself. Han et al. (2015)
254 concluded that a hypothetical scenario such as the breaking of a dam – which they used to start
255 their erosion model simulations – provides a stable and consistent release method. Deubelbeiss et
256 al. (2010 and 2011), for a case study in the Swiss Alps, suggested that the block release method is
257 most appropriate method for small to moderate initial volumes ranging from 1 m³ up to 100 m³
258 using the RAMMS debris flow model. The alternative release method using a discharge
259 hydrograph seems to be more suitable for larger initial volumes (Deubelbeiss et al., 2010 and 2011)
260 (> 100 m³) which – in general – might be plausible for the larger channel of the Bondasca
261 catchment.

262 The main problem with the block release is that the initial flow depth, width, or length of the initial
263 landslide can be unrealistically large in comparison to field observations. Users have to resort to
264 such large initial landslide volumes because most models do not allow for erosion along the



265 channel path. The total debris flow volume, typically measured in the deposition zone, is often used
266 as the initial landslide volume, thereby implicitly ignoring the possibility that channel-bed erosion
267 and flow bulking occur (Frank et al., 2015). The input hydrograph starting condition in RAMMS
268 was intended to help circumvent this problem by allowing users to specify an influx of debris as a
269 function of time at a point lower in the watershed (e.g. just above the fan apex).
270 The block release volume is calculated by defining a specific block release height (with a precision
271 of 1 cm) based on a pre-defined release area. The model assumes an instantaneous failure of the
272 landslide. The initial landslide surface elevation is then set to the initial elevation of the land
273 surface using an automatic procedure in RAMMS (the “subtract release from DTM” option in
274 RAMMS introduced in version 1.6.45). The main advantage of this procedure is that it prevents
275 unrealistic lateral spreading of the initial landslide mass in comparison with a landslide “block”
276 situated on top of the land surface.

277 3.3.3. Specified erosion rates

278 As a basis for comparison of the sensitivity of the erosion algorithm, we hold constant the default
279 erosion model coefficients (critical shear stress τ_c , potential erosion depth as a function of basal
280 shear stress $\frac{dz}{dt}$, erosion rate $\frac{dz}{dt}$) described above. In the previous study (Frank et al., 2015) we
281 demonstrated that an erosion rate of $\frac{dz}{dt} = 2.5 \text{ cm s}^{-1}$ based on field data from the Illgraben
282 catchment, Switzerland (Berger et al., 2011) produces plausible results for the much steeper
283 Spreitgraben catchment. The catchments described in this paper are different in size and slope, so
284 one might expect some variation in erosion rate. However, the erosion algorithm in RAMMS
285 allows for rates up to $\frac{dz}{dt} = 5.0 \text{ cm s}^{-1}$, with an option to include a shape file describing where
286 erosion may occur e.g. to account for engineering structures such as check dams or sills, or natural
287 features such as bedrock, where significant erosion is not expected during one debris-flow event.
288 For comparison we also used a rate of $\frac{dz}{dt} = 1.25 \text{ cm s}^{-1}$ based on a lower rate from Berger et al.
289 (2011).

290 4. Erosion and entrainment: observations and modeling results

291 4.1. Erosion patterns and entrainment model calibration

292 The observed erosion patterns are the basis for calibrating the RAMMS model coefficients, in
293 particular the friction coefficients ξ and μ are systematically adjusted in successive model runs,
294 until a satisfactory model result is achieved. The erosion pattern is derived by assessing the
295 difference between the digital elevation models. In both study areas, a measured erosion pattern
296 caused by one single debris flow event is not available. We therefore focus on the spatial



297 distribution of erosion and deposition, instead of attempting to exactly predict the spatial change
298 due to the debris flow process.

299 In the Meretschibach, the change in the DTM includes the erosion due to three debris flow events
300 which appear to have originated on an open-slope talus deposit (Figure 3A). The location of the
301 release area at the Meretschibach corresponds to the upper most visible erosion scar visible in the
302 DTM analysis and as described above includes the erosion due to three debris flow events between
303 July 17 to October 28, 2014 (Fig. 3A). Therefore, the release area was placed within the channel,
304 where up to 2.5 meters of erosion was observed (upper end of the blue polygon at about 1750 m
305 a.s.l. in Fig. 3A.). The location is just below a bedrock step intersecting the main channel at about
306 1800 m a.s.l. Further monitoring at the upper Bochtür subcatchment using interval cameras and
307 conducting field observations on the site itself confirmed that at least some of the debris flows most
308 likely initiated at this location.

309 We calibrated the RAMMS model using an initial block release volume of 10 m^3 which
310 corresponds to the channel depth of 1-2 m and a width of 2-4 m at this location. To keep the initial
311 volume within the channel and prevent unrealistic lateral outflow, no-flux boundaries were created
312 at the lateral sides of the initial landslide block. Within the middle and lower channel sections (Fig.
313 3A, blue polygon), the observed runout and relative erosion patterns can be best reproduced using
314 Voellmy friction parameters $\xi = 200 \text{ ms}^{-2}$ and $\mu = 0.6$ (Fig. 3B2). The modeled velocities of
315 $6\text{-}9 \text{ ms}^{-1}$ using $\xi = 200$ are plausible, although independent field data are not available for
316 comparison. The parameter combination $\xi = 200 \text{ ms}^{-2}$ and $\mu = 0.7$ results in overbank flow along
317 both sides of the middle channel, which was not observed in the field (Fig. 3C2). There were
318 neither deposits outside of the channel nor were levees deposited along this entire channel reach
319 (Fig. 3A, blue polygon). In contrast, the erosion pattern using $\xi = 200 \text{ ms}^{-2}$ and $\mu = 0.5$ resulted in
320 an even distribution of erosion along the entire channel length, which is inconsistent with the field
321 results which showed locations of deeper erosion depths (Fig. 3A). Within the normal range of the
322 ξ parameter (Bartelt et al., 2013) the differences in flow and erosion patterns were small in
323 comparison to those resulting from variations in μ , and are therefore not described herein. Hence,
324 the further model runs were conducted using the best-fit parameters $\xi = 200 \text{ ms}^{-2}$ and $\mu = 0.6$ in the
325 sensitivity analyses described in subsequent sections.

326 In the Bondasca catchment, the differential elevation model includes both the rock avalanche
327 deposit (27 December 2011) and the erosion due to one debris-flow event (5 July 5, 2012) (Fig. 5).
328 The upper end of channel erosion is located just below a planar outcrop of bedrock (Fig. 4B)
329 corresponding to the likely location debris flow initiation zone (Fig. 5C). The surface runoff
330 channels along the west side of the wall and runoff across the wall surface (Fig. 4B) converge on
331 the sediments at the bottom of the rock wall (see pictures from 2014 in Fig. 5). This scenario
332 suggests a firehose-type debris-flow initiation (e.g. Godt and Coe, 2007). Hence, this location was
333 used for the runout modeling.



334 The observed erosion along the main debris flow channel (Fig. 5C) – resulting from the two debris
335 flow events in July 2012 – were used to calibrate the RAMMS model within the upper two thirds of
336 the study reach (Figure 4B, brown polygon) by varying the model parameters ξ and μ . The best fit
337 was found with the parameter combination $\xi = 400 \text{ ms}^{-2}$ and $\mu = 0.3$. However, the observed
338 elevation change also includes secondary processes such as lateral bank collapse and the deposits
339 of debris-flow snouts and levees within the channel. Channel sections where the events eroded into
340 the deposits present can also be identified by the stratigraphy in the field.

341 **4.2. Entrainment modeling and runout patterns**

342 The runout of a (landslide-type) block release of 10 m^3 , neglecting erosion (Fig. 6A) results in
343 maximum flow heights smaller than 0.5 m and the flow stops in the channel upstream of the
344 deposition zone. By contrast, including debris-flow erosion (Fig. 6B) leads to a more realistic flow
345 pattern consisting of flow within the channel reaching the deposition zone without any lateral
346 outflow. For comparison, if the total event volume ($\approx 1,555 \text{ m}^3$) is released as a landslide and the
347 debris-flow is not allowed to erode the channel (Fig. 6C), the runout shows overbank flow along
348 the upper channel reaches below the initiation area. The last scenario is a typical example of how
349 debris-flow runout models are used when the total event volume is known. These results illustrate
350 the ability of the runout model to better predict the erosion pattern if the channel-bed erosion and
351 bulking process is included in the model.

352 **4.3. Erosion model sensitivity testing**

353 The results show that the total volume of eroded sediment, at both field sites, depends strongly on
354 the initial landslide volume. At both the Meretschibach and the Bondasca catchments, there is a
355 strong increase in the amount of sediment entrained and consequent increase in debris-flow volume
356 (Fig. 7) for relatively small increases of the initial landslide volume. At the Meretschibach
357 catchment, the erosion model – using the default maximum erosion rate $\frac{dz}{dt} = 2.5 \text{ cm s}^{-1}$ – shows the
358 highest sensitivity to the total erosion volume between 2 and 3 m^3 of initial block release (e.g.
359 initial landslide volume). Above $4\text{-}5 \text{ m}^3$ of initial block volume the increase of the total erosion
360 volume within the erosion domain remains approximately constant. The cause for the rapid
361 increase is related to the critical shear stress in the entrainment algorithm. Small initial landslides
362 do not generate enough shear stress to initiate erosion, whereas larger landslides can cause erosion
363 over the entire computational domain.

364 If we double the erosion rate to $\frac{dz}{dt} = 5.0 \text{ cm s}^{-1}$ based on field estimates reported by Frank et al.,
365 2015 for the Spreitgraben catchment, a similar pattern is observed in the relationship between total
366 erosion volume as a function of initial release volume. However the erosion volumes are 3 to 5
367 times larger than the ones resulting from the default erosion rate at the same initial release volume.



368 In contrast, implementing only half the default maximum erosion rate ($\frac{dz}{dt} = 1.25 \text{ cm s}^{-1}$) for low
369 erosion scenarios decreases the sensitivity to initial volume in an analogous manner.
370 Similar trends in total erosion volume as a function of initial block release (landslide) volume are
371 observed at the Bondasca catchment. However, the model only starts to predict significant erosion
372 volumes for block releases exceeding 20 m^3 , and the progressive increase in total erosion volume
373 as a function of initial block release volume is somewhat less steep. For the default erosion rate $\frac{dz}{dt}$
374 $= 2.5 \text{ cm s}^{-1}$ (Frank et al., 2015), total erosion volumes increase most strongly between initial
375 volumes of 20 to 100 m^3 . The topography at the Bondasca catchment is somewhat less steep and
376 more variable, which may help explain these differences. Doubling the default erosion rate at the
377 Bondasca catchment results in the onset of erosion for initial volumes between 20 and 30 m^3 . When
378 reducing the default erosion rate to half of the default value, the erosion model depicts a somewhat
379 less sensitive reaction of the erosion model than using the default rate.

380 5. Discussion

381 The total erosion volumes observed in the sensitivity tests (Fig. 7) indicate a strong sensitivity to
382 block release volume (initial landslide volume) over a relatively narrow range of block release
383 volumes. This result is based on the assumption that the entire landslide fails instantaneously and
384 not progressively as a sequence of smaller landslides over a longer period of time. Information on
385 the style of initial landslide failure are not available for either field site, therefore we focus the
386 discussion on other factors related to the runout modeling. One striking difference between the two
387 field sites is that the size of the block release necessary to cause significant erosion is an order of
388 magnitude larger at the Bondasca site. The channel cross-sectional area where the flow travels and
389 therefore where the erosion model is active is different at the two field sites. The Meretschibach is
390 substantially steeper (50 to 65% vs. 15 to 35%). This results in larger shear stresses at the
391 Meretschibach for the same initial landslide thickness, because the shear-stress varies as the
392 product of initial release thickness, flow density, and channel slope. Other factors such as
393 differences in channel-bed roughness may also be important, however the Voellmy friction relation
394 within RAMMS does not explicitly consider channel-bed roughness.

395 In the RAMMS debris flow model, the development of the flow properties is controlled by the
396 Voellmy friction parameters ξ and μ (described in section 3.1) where ξ is the dominant control over
397 the flow velocities when the flow is moving rapidly and μ controls the runout distance. The ξ
398 parameter was found in this study to have a relatively small influence over the flow behavior in
399 comparison with the Coulomb friction term μ . The RAMMS manual (Bartelt et al., 2013) suggests
400 using the tangent of the fan slope as first estimate to determine μ . As described in the calibration
401 procedure (section 3.2), this corresponds to relative erosion patterns measured by differential DTM
402 analysis. Hence, we conclude that the tangent of the channel slope can be used as a first approach



403 to define parameter μ also for the erosion model, which was also found to be useful by Frank et al.
404 (2015) in the first application of the model.
405 Morphological effects influence the erosional behavior of the field data based erosion model. The
406 Bondasca channel is more variable in width and planform direction compared to the comparably
407 uniform and straight Meretschibach channel. This difference will cause larger spatial variability in
408 shear stress at Bondasca channel and therefore the channel will have a more variable onset of
409 debris flow erosion along the length of the channel. In the Bondasca catchment, the channel where
410 erosion takes place is significantly wider (4-10 m) than in the Meretschibach (1-3 m). On the one
411 hand, the flow can laterally spread more often in Bondasca than in the Meretschibach, thereby
412 locally reducing flow height, shear stresses and maximum potential erosion depth. On the other
413 hand, once the critical shear stress is exceeded, the potential erosion depth tends to increase more
414 rapidly in a narrow channel such as in the Meretschibach channel.
415 Another difference between the Meretschibach and the Bondasca channels is that the Bondasca
416 channel bed has a rougher surface with more scours holes, and larger blocks within the channel
417 which are similar in size to the nominal width of the channel. The model does not consider local
418 variations in erodibility due to the presence of large blocks, so local scour patterns in the field
419 around the large blocks are not present in the model results. Prancevic and Lamb, (2015a)
420 suggested that in rough mountain channels the large particles can be interlocked and hence more
421 stable. In contrast, local concentration of the flow between such large blocks may cause locally
422 very large shear stresses and corresponding large erosion rates. However, we do not have enough
423 information on the mobility of the large blocks, so this question cannot be addressed in more detail
424 herein.
425 The current version of the RAMMS model with erosion (version 1.6.45) does not adjust the
426 elevation of the bed when erosion occurs. The erosion can be subtracted from the initial DTM as a
427 post-processing step within the user interface, e.g. for modeling subsequent surges. This issue was
428 discussed at length by Frank et al (2015), and it can potentially complicate the interpretation of
429 erosion patterns resulting from multiple debris flows. Insufficient field data are available to help
430 constrain the events described herein.
431 Further assessment of the relation of the total erosion volumes depending on the initial volumes can
432 be made by calculating a bulking factor. The bulking factor BF is the ratio between the total
433 erosion volume V_{ero} to the initial volume V_{ini} :

$$434 \quad BF = V_{ero}/V_{ini} \quad (8)$$

435 At the Meretschibach channel, the bulking factor is ≈ 200 when the erosion model using the default
436 erosion rate and an initial volume of 3 m^3 (Fig. 8). The BF reaches a peak $BF_p \approx 300$ at a release
437 volume of 4 m^3 . It then drops to a $BF \approx 30$ for an initial volume of 100 m^3 . The model simulations
438 using the doubled default erosion rate show a bulking factor peak $BF_p \approx 1,800$ for an initial release



439 volume of 2 m^3 ; half the default erosion rate shifts this peak to 50 m^3 for the initial volume but the
440 corresponding peak bulking factor drops significantly down to ≈ 14 .

441 The behavior of the bulking factor for the default erosion rate at the Bondasca catchment is
442 relatively smooth when compared to that at the Meretschibach. A peak bulking factor can be
443 identified somewhere between 200 and 500 m^3 but the value is lower in comparison (≈ 11) for the
444 default erosion rate. The doubled rate leads to a peak bulking factor BF_p of ≈ 700 at a release
445 volume of 30 m^3 . That is still large compared to examples in the literature (BF from 10 to 50
446 reported by Berti et al., 1999 and Vandine and Bovis, 2002). Nevertheless, a several hundred fold
447 increase of the debris flow volume due to bulking is plausible for extreme erosion cases. Larger
448 erosion rates might be expected for pyroclastic deposits (not present in the catchments described
449 herein) or due to the presence of very recent rock avalanche deposits which may contain firn-ice-
450 debris mixtures (e.g. Spreitgraben, Tobler et al., 2014; Frank et al., 2015). Large erodibilities may
451 be expected at the Bondasca catchment because the rock avalanche event occurred during winter
452 and may have contained significant amount of snow.

453 Due to the very long ($\approx 4 \text{ km}$) and flat ($\approx 15\%$) channel section in the middle segment of the
454 Bondasca catchment, the estimated deposition volumes ($\approx 40,000 \text{ m}^3$) above the inlet of the
455 Bondasca river in the central valley are highly influenced by further erosional and depositional
456 processes along the channel.

457 6. Conclusion

458 Debris-flow runout predictions can be improved when considering the increase in flow volume
459 along the flow path. Using a recently-introduced empirical erosion algorithm within the RAMMS
460 2D runout model (Frank et al., 2015) we illustrate that runout patterns at the Meretschibach and
461 Bondasca catchments, in Switzerland, can be accurately modeled. When calibrated with field data,
462 the model produces more realistic runout patterns compared to simulations which do not consider
463 entrainment and bulking. In particular, we could show that even in very steep ($\approx 60\text{--}65\%$) and
464 narrow (4–6 m) torrent channels, lateral overflow – not observed in the field case – is prevented
465 when applying the entrainment model. However the model results can be quite sensitive to the
466 volume of the initial block release in the model which corresponds to the initial landslide volume.
467 The predicted erosion volumes are sensitive to the initial debris flow volume, with bulking factors
468 approaching 2000 predicted by the model, depending on the scenario considered. However, the
469 results are also sensitive to slope angle and channel morphology. The two field sites differ
470 substantially: the Meretschibach catchment is very steep with a straight and narrow channel,
471 whereas the Bondasca channel is less steep but morphologically more complex, yet the calibration
472 procedure is the same as for the standard RAMMS model which does not include the entrainment
473 process. The overall method presented herein is useful for case studies where sufficient data are



474 available to constrain the model results. However, more case studies have to be conducted to
475 develop a more comprehensive recommendation for modeling the runout of erosive debris flows in
476 natural terrain.

477 **Acknowledgements**

478 This project was partially supported by the CCES-TRAMM project. We are grateful to Christian
479 Huggel for helpful discussions and comments. We thank Martin Keiser of Amt für Wald und
480 Naturgefahren of Canton Graubünden for providing elevation data for the Bondasca catchment and
481 Ruedi Bösch, WSL, for the elevation data at the Meretschibach catchment.



482 **References**

- 483 Beguería, S., Van Asch, Th. W. J., Malet, J.-P., and Gröndahl, S.: A GIS-based numerical model
484 for simulating the kinematics of mud and debris flows over complex terrain, *Nat. Hazards Earth*
485 *Syst. Sci.*, 9, 1897–1909, doi:10.5194/nhess-9-1897-2009, 2009.
- 486 Bartelt, P., Buehler, Y., Christen, M., Deubelbeiss, Y., Graf, C., and McArdell, B. W.: RAMMS –
487 rapid mass movement simulation, A modeling system for debris flows in research and practice,
488 user manual v1.5, debris flow, manuscript update: 31 January 2013, WSL Institute for Snow
489 and Avalanche Research SLF, available at:
490 http://ramms.slf.ch/ramms/downloads/RAMMS_DBF_Manual.pdf (last access: 27 February
491 2015), 2013.
- 492 Benda, L.: The influence of debris flows on channels and valley floors in the Oregon Coast Range,
493 USA. *Earth Surf. Proc. Landf.* 15, 457-466, 1990.
- 494 Berger, C., McArdell, B.W., and Schlunegger, F.: Sediment transfer patterns at the Illgraben
495 catchment, Switzerland: Implications for the time scales of debris flow activities,
496 *Geomorphology*, 125, 421–432, 2010.
- 497 Berger, C., McArdell, B. W., and Schlunegger, F.: Direct measurement of channel erosion by
498 debris flows, Illgraben, Switzerland, *J. Geophys. Res.*, 116, F01002,
499 doi:10.1029/2010JF001722, 2011.
- 500 Berti, M.; Genevois, R.; Simoni, A. and Tecca, P.R.: Field observations of a debris flow event in
501 the Dolomites. *Geomorphology*, 29:265–274, 1999.
- 502 Breien, H., De Blasio, F. V., Elverhøi, A & Høeg, K. Erosion and morphology of a debris flow
503 caused by a glacial lake outburst flood, western Norway. *Landslides* 5, 271-280, 2008.
- 504 Cannon, S. H. and Reneau S. L.: Conditions for generation of fire-related debris flows, Capulin
505 Canyon, New Mexico, *Earth Surf. Processes Landforms*, 25(10), 1103-1121, 2000.
- 506 Christen, M., Kowalski, J., and Bartelt, P.: RAMMS: Numerical simulation of dense snow
507 avalanches in three-dimensional terrain, *Cold Reg. Sci. Technol.*, 63, 1–14, 2010.
- 508 Christen, M., Bühler, Y., Bartelt, P., Leine, R., Glover, J., Schweizer, A., Graf, C., McArdell, B.
509 W., Gerber, W., Deubelbeiss, Y., Feistl, T., and Volkwein, A.: Integral hazard management
510 using a unified software environment: numerical simulation tool “RAMMS” for gravitational
511 natural hazards, edited by: Koboltschnig, G., Hübl, J., Braun, J., 12th Congress
512 INTERPRAEVENT, 23–26 April 2012 Grenoble, France, Proceedings, Vol. 1, Klagenfurt,
513 International Research Society INTERPRAEVENT, 77–86, 2012.
- 514 Crosta, G. B., Imposimato, S., and Roddeman, D. G.: Numerical modelling of large landslides
515 stability and runout, *Nat. Hazards Earth Syst. Sci.*, 3, 523–538, doi:10.5194/nhess-3-523-2003,
516 2003.



- 517 D'Ambrosio, D., Di Gregorio, S., and Iovine, G.: Simulating debris flows through a hexagonal
518 cellular automata model: SCIDDICA S3-hex, Nat. Hazards Earth Syst. Sci., 3, 545–559,
519 doi:10.5194/nhess-3-545-2003, 2003.
- 520 Deubelbeiss, Y.; Graf C.; McArdell, B.; Bartelt, P.: Numerical modeling of debris flows – Case
521 study at Dorfbach, Randa (VS), Swiss Geoscience Meeting. Fribourg, 2010.
- 522 Deubelbeiss, Y.; Graf, C.; McArdell, B.; Bartelt, P. Numerical modeling of debris flows – Case
523 study at Dorfbach, Randa (Valais, Switzerland). Geophysical Research Abstracts Vol. 13,
524 EGU2011-5681, EGU General Assembly 2011, Vienna, 2011.
- 525 Deubelbeiss, Y. and McArdell, B. W.: Dynamic modelling of debris-flow erosion and deposition
526 with application to the USGS debris flow flume experiments, Geophys. Res. Abstr. 14,
527 EGU2012-7906, 2012.
- 528 Dietrich, W. E., and Dunne, T.: Sediment budget for a small catchment in mountainous terrain, *Z.*
529 *Geomorphology*, 29, 191-206, 1978.
- 530 Fannin, R. J. and Wise, M. P.: An empirical_statistical model for debris flow travel distance. *Can.*
531 *Geotech. J.* 38, 982-994, 2001.
- 532 Fankhauser F., Lucas Guzman D. R. Oggier N., Maurer H., Springman S. M. 2015. Seasonal
533 Response and Characterization of a Scree Slope and Active Debris Flow Catchment Using
534 Multiple Geophysical Techniques: The case of the Meretschibach Catchment, Switzerland.
535 Geophysical Research Abstracts Vol. 17, EGU2015-PREVIEW, EGU General Assembly 2015,
536 2015.
- 537 Frank, F., McArdell, B. W., Huggel, C., and Vieli, A.: The importance of entrainment and bulking
538 on debris flow runout modeling: examples from the Swiss Alps, Nat. Hazards Earth Syst. Sci.,
539 15, 2569-2583, doi:10.5194/nhess-15-2569-2015, 2015.
- 540 Frank, F., McArdell, B. W., Huggel, C., and Vieli, A.: Sediment input and debris flow system
541 activity cycles - an analysis of the development in different catchments in Switzerland. In prep.
- 542 Gabus, J. H., Weidmann, M., Bugnon, P.-C., Burri, M., Sartori, M., and Marthaler, M.: Geological
543 map of Sierre, LK 1278, sheet 111, scale 1:25,000, in Geological Atlas of Switzerland, Swiss
544 Geol. Surv., Bern, Switzerland, 2008.
- 545 Gallino, G. L., and Pierson, T. C.: The 1980 Polallie Creek debris flow and subsequent dam-break
546 flood, East Fork Hood River Basin, Oregon, U.S. Geol. Surv. Open File Rep., 84-578, 37 pp.,
547 1984.
- 548 Gamma, P.: "dfwalk" Ein Murgang-Simulationsmodell zur Gefahrenzonierung. Institute of
549 Geography, University of Berne. Geographica Bernensia G66 (only available in German), 2000.
- 550 Gartner, J. E., Cannon, S. H., Santi, P. M. and Dewolfe, V. G.: Empirical models to predict the
551 volumes of debris flows generated by recently burned basins in the western U.S.,
552 *Geomorphology*, 96(3-4), 339-354, 2008.



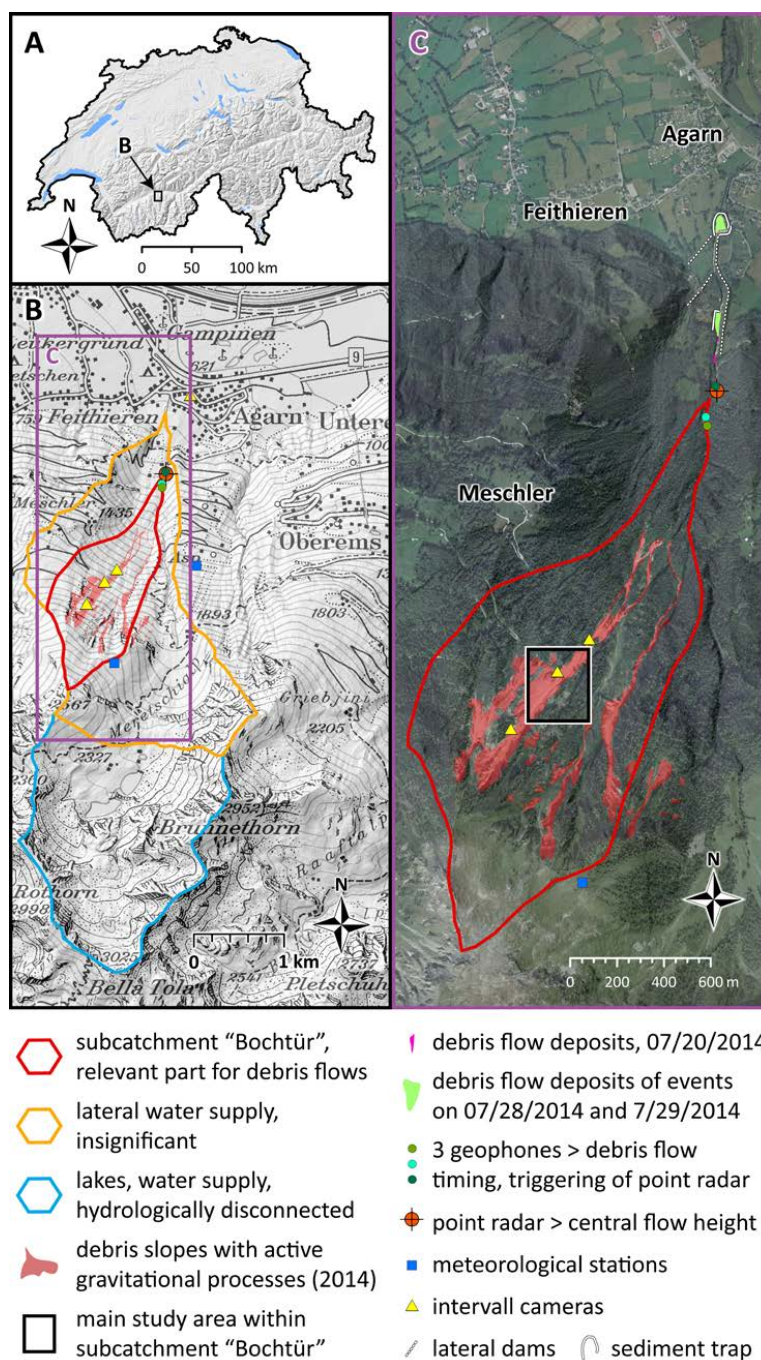
- 553 Godt, Jonathan W. and Coe, Jeffrey A.: Alpine debris flows triggered by a 28 July 1999
554 thunderstorm in the central Front Range, Colorado, *Geomorphology*, Volume 84, Issues 1–2,
555 Pages 80-97, ISSN 0169-555X, <http://dx.doi.org/10.1016/j.geomorph.2006.07.009>. 15 February
556 2007.
- 557 Guthrie, R. H., Hockin, A., Colquhoun, L., Nagy, T., Evans, S.G. and Ayles, C.: An examination
558 of controls on debris flow mobility: Evidence from coastal British Columbia. *Geomorphology*
559 114, 601-613, 2010.
- 560 Han, Zheng; Chen, Guangqi; Li, Yange; Tang, Chuan; Xu, Linrong; He, Yi; Huang, Xun; Wang,
561 Wei: Numerical simulation of debris-flow behavior incorporating a dynamic method for
562 estimating the entrainment, *Engineering Geology*, Volume 190, Pages 52-64, ISSN 0013-7952,
563 14 May 2015, available at: <http://dx.doi.org/10.1016/j.enggeo.2015.02.009> (last access: 10
564 February 2016), 2015.
- 565 Hohermuth, B. and Graf, C.: Einsatz numerischer Murgangsimulationen am Beispiel des integralen
566 Schutzkonzepts Plattenbach Vitznau. *Wasser Energ. Luft* 106, 4: 285-290, available at:
567 <http://www.wsl.ch/wsl/info/mitarbeitende/grafc/pdf/14138.pdf> (last access: 10 February 2016),
568 2014.
- 569 Hungr, O., McDougall, S. and Bovis, M.: Entrainment of material by debris flows, in *Debris-Flow*
570 *Hazards and Related Phenomena*, edited by M. Jakob and O. Hungr, pp. 135-158, Springer,
571 New York, 2005.
- 572 Hungr, O., Morgan, G. C. and Kellerhals, R.: Quantitative analysis of debris torrent hazards for
573 design of remedial measures, *Can. Geotech. J.*, 21(4), 663-677, 1984.
- 574 Hungr, O. and McDougall, S.: Two numerical models for landslide dynamic analysis, *Comput.*
575 *Geosci.*, 5, 978-992, 2009.
- 576 Hussin, H. Y., Quan Luna, B., van Westen, C. J., Christen, M., Malet, J.-P., and van Asch, Th. W.
577 J.: Parameterization of a numerical 2-D debris flow model with entrainment: a case study of the
578 Faucon catchment, Southern French Alps, *Nat. Hazards Earth Syst. Sci.*, 12, 3075-3090,
579 doi:10.5194/nhess-12-3075-2012, 2012.
- 580 Iverson, R. M.: *The Physics of Debris Flows*: IN: *Reviews of Geophysics*, 35, 3, August 1997, p.
581 245-296, published by Geophysical Union, Paper # 97RG00426, 1997.
- 582 Iverson, R.M., Reid, M.E., Logan, M., LaHusen, R.G., Godt, J.W. and Griswold, J.G.: Positive
583 feedback and momentum growth during debris-flow entrainment of wet bed sediment. *Nature*
584 *Geoscience* v. 4, no. 2, p. 116-121. doi: 10.1038/NGEO1040, 2011.
- 585 Iverson, R.M., Reid, M.E., Logan, M., LaHusen, R.G., Godt, J.W., and Griswold, J.G.: Positive
586 feedback and momentum growth during debris-flow entrainment of wet bed sediment. *Nature*
587 *Geoscience* v. 4, no. 2, p. 116-121. doi: 10.1038/NGEO1040, 2011.
- 588 May, C. L.: Debris flows through different forest age classes in the Central Oregon Coast Range, J.
589 *Am. Water Resour. Assoc.*, 38(4), 1097-1113, 2002.



- 590 McCoy, S. W., Kean, J. W., Coe, J. A., Tucker, G. E., Staley, D. M. and Wasklewicz, T. A.:
591 Sediment entrainment by debris flows: In situ measurements from the headwaters of a steep
592 catchment, *J. Geophys. Res.*, 117, F03016, doi:10.1029/2011JF002278, 2012.
- 593 Medina, V., Hürlimann, M., and Bateman, A.: Application of FLATModel a 2-D finite volume
594 code, to debris flows in the northeastern part of the Iberian Peninsula, *Landslides*, 5, 127–142,
595 2008.
- 596 Meyer, G. A., and Wells, S. G.: Fire-related sedimentation events on alluvial fans, Yellowstone
597 National Park, USA, *J. Sediment. Res.*, 67(5), 776–791, 1997.
- 598 Oggier, N. and McArdell, B. W.: Ereignisanalyse - Murgangereignisse Meretschibach 20./28./29.
599 Juli 2014. Birmensdorf, 21. Januar 2015, (only available in German), 2015a.
- 600 Oggier, N. and Bösch, R.: Zwischenbericht, Drohnenflug Meretschibach 28. Oktober 2014,
601 Birmensdorf, 26. Februar 2015, (only available in German), 2015b.
- 602 Pierson, T. C., Janda, R. J., Thouret, J.-C. and Borrero, C. A.: Perturbation and melting of snow and
603 ice by the 13 November 1985 eruption of Nevado del Ruiz, Colombia, and consequent
604 mobilization, flow and deposition of lahars. *J. Volcanol. Geotherm. Res.* 41, 17–66, 1990.
- 605 Prancevic, J. P., and Lamb, M. P.: Particle friction angles in steep mountain channels, *J. Geophys.*
606 *Res. Earth Surf.*, 120, doi:10.1002/2014JF003286, 2015a.
- 607 Prancevic, J. P., and M. P. Lamb: Unraveling bed slope from relative roughness in initial sediment
608 motion, *J. Geophys. Res. Earth Surf.*, 120, doi:10.1002/2014JF003323, 2015b.
- 609 Procter, J., Cronin, S. J., Fuller, I. C., Lube, G. and Manville, V.: Quantifying the geomorphic
610 impacts of a lake-breakout lahar, Mount Ruapehu, New Zealand, *Geology*, 38(1), 67–70, 2010.
- 611 Revellino, P., Hungr, O., Guadagno, F. M. and Evans, S. G.: Velocity and runout simulation of
612 destructive debris flows and debris avalanches in pyroclastic deposits, Campania region, Italy,
613 *Environ. Geol.*, 45(3), 295–311, 2004.
- 614 Scheingross, J. S., Winchell, E. W., Lamb, M. P. and Dietrich, W. E.: Influence of bed patchiness,
615 slope, grain hiding, and form drag on gravel mobilization in very steep streams, *J. Geophys.*
616 *Res. Earth Surf.*, 118, 982–1001, doi:10.1002/jgrf.20067, 2013.
- 617 Scheuner, T., Keusen, H., McArdell, B. W., and Huggel, C.: Murgangmodellierung mit dynamisch-
618 physikalischem und GIS-basiertem Fliessmodell, Fallbeispiel Rotlauigraben, Guttannen, August
619 2005, *Wasser Energie Luft*, 101: 15–21 (only available in German), 2009.
- 620 Scheuner, T., Schwab, S., and McArdell, B. W.: Application of a two-dimensional numerical
621 model in risk and hazard assessment in Switzerland, in 5th DFHM, Padua, Italy, 2011.
- 622 Schürch, P., Densmore, A. L., Rosser, N. J., and McArdell, B. W.: Dynamic controls on erosion
623 and deposition on debris-flow fans, *Geology*, 39, 827–830, 2011.
- 624 Scott, K. M., Vallance, J. W., Kerle, N., Macias, J. L. Strauch, W. and Devoli, G.: Catastrophic
625 precipitation-triggered lahar at Casita volcano, Nicaragua: Occurrence, bulking and
626 transformation, *Earth Surf. Processes Landforms*, 30(1), 59–79, doi:10.1002/esp.1127, 2005.



- 627 Suwa, H., and Okuda, S.: Dissection of valleys by debris flow, *Z. Geomorphology*, 35, 164-182,
628 1980.
- 629 Szymczak, S., Bollschweiler, M., Stoffel, M. and Dikau, R.: Debris-flow activity and snow
630 avalanches in a steep watershed of Valais Alps (Switzerland): Dendrogeomorphic event
631 reconstruction and identification of triggers. *Geomorphology* 116, 107-114, 2010.
- 632 Tobler, D., Kull, I., Jacquemart, M., and Haehlen, N.: Hazard Management in a Debris Flow
633 Affected Area: Case Study from Spreitgraben, Switzerland, *Landslide Science for a Safer
634 Geoenvironment*, 3, 25–30, doi:10.1007/978-3-319-04996-0_5, 2014.
- 635 Vallance, J. W. and Scott, K. M.: The Osceola Mudflow from Mount Rainier: Sedimentology and
636 hazard implications of a huge clay-rich debris flow, *Geol. Soc. Am. Bull.*, 109(2), 143-163,
637 1997.
- 638 Vandine, D.F. and Bovis M.: History and goals of Canadian debris-flow research, a review. *Nat
639 Hazards* 26:69–82, 2002.
- 640 Wang, G., Sassa, K. and Fukuoka, H.: Downslope volume enlargement of a debris slide_debris
641 flow in the 1999 Hiroshima, Japan, rainstorm. *Eng. Geol.* 69, 309-330, 2003.

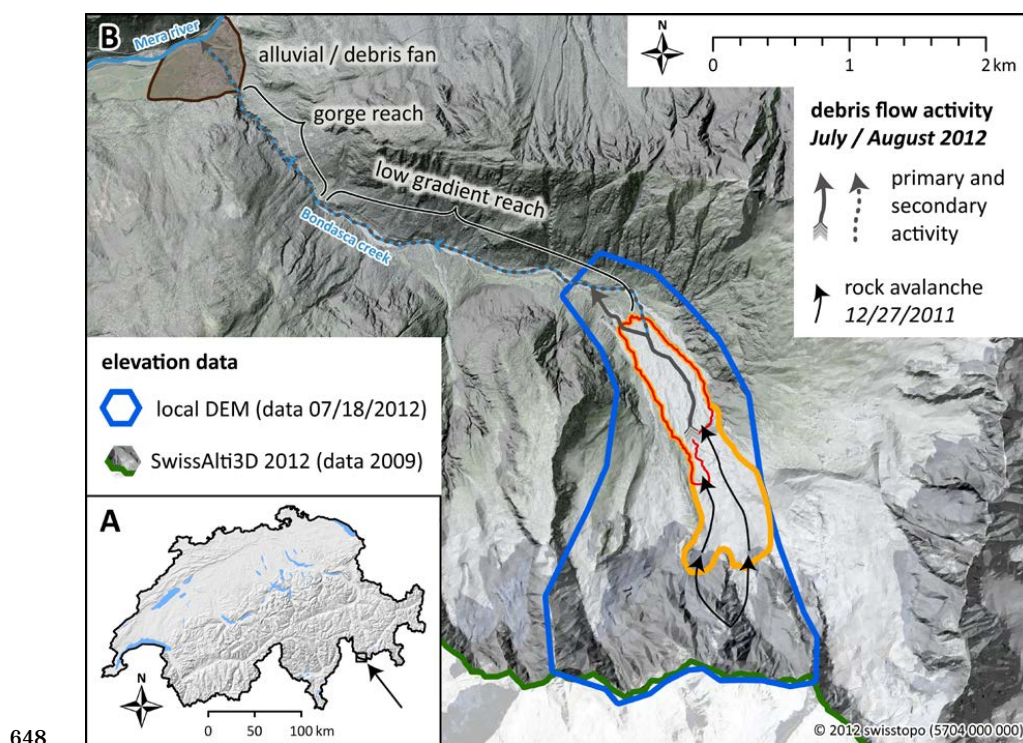


642

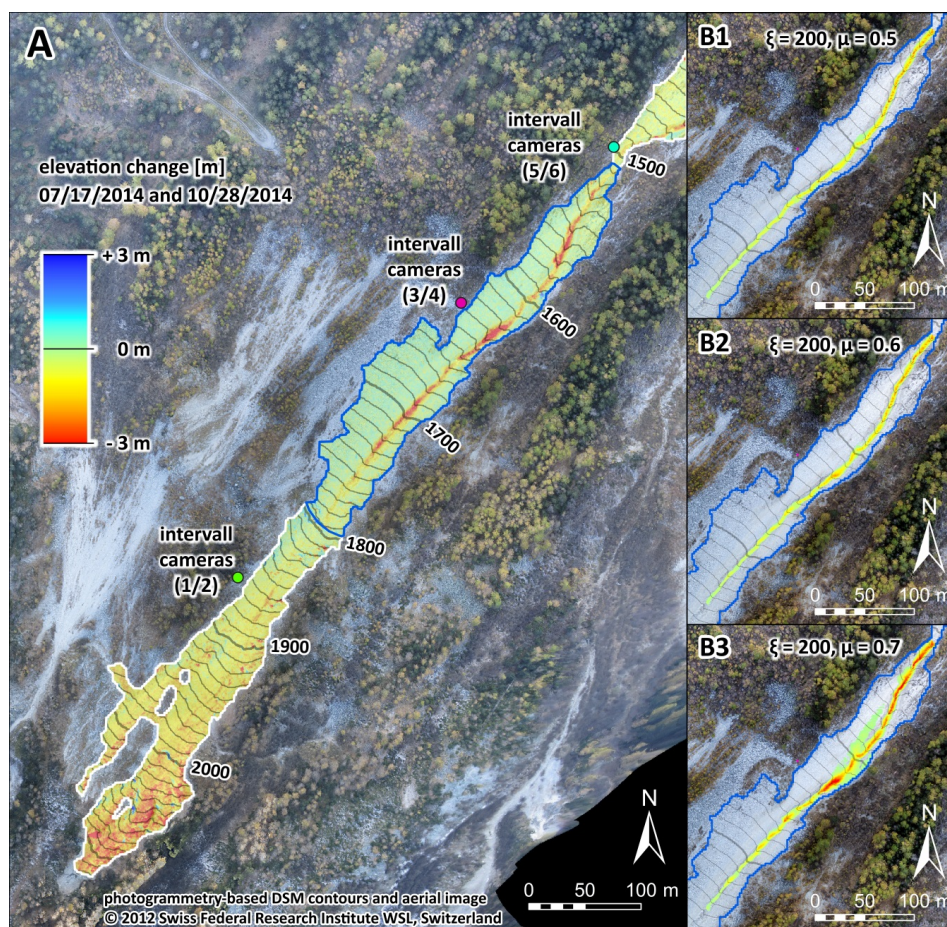
643 **Figure 1.** **A.** Location of the Meretschibach catchment in Southern Switzerland. **B.** Subcatchments
 644 of the Meretschibach and locations of the instrumentation site and data available for the erosion
 645 model analyses **C.** Initiation zone of the July 2014 events and camera positions. The main study



646 channel reach for the model testing is located in the middle part of “Bochtür” (black-white
647 retangle), swissimage©2014, swisstopo (5704 000 000) (2014).

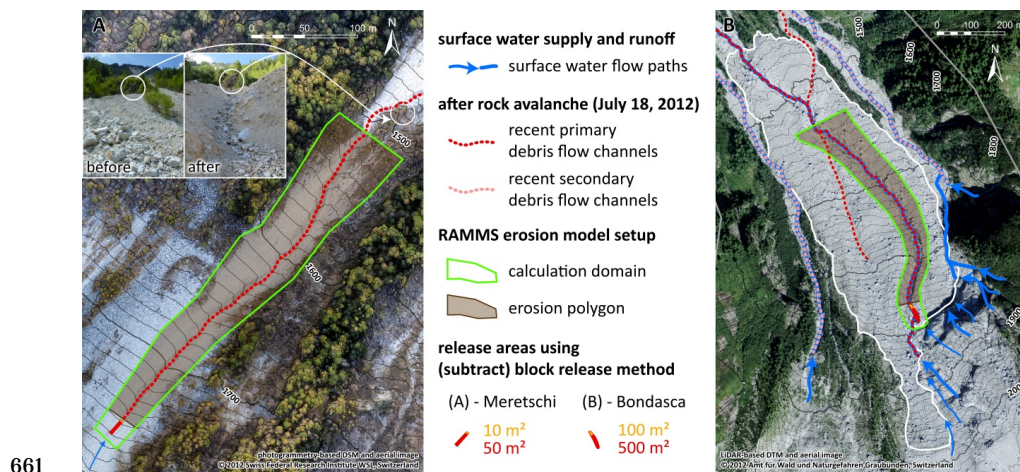


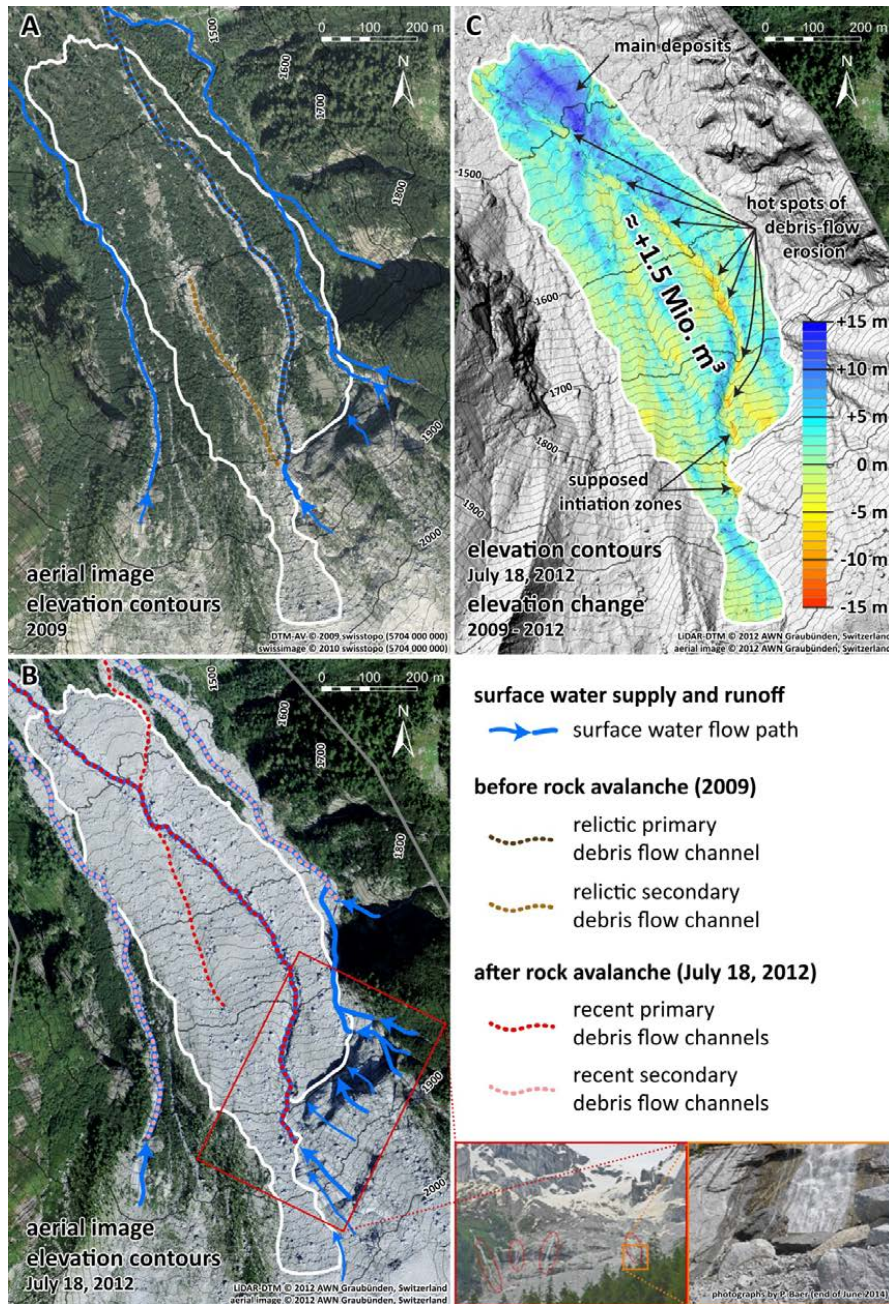
649 **Figure 2.** A. Location of the Bondasca catchment in south-eastern Switzerland close to the border
650 to Italy. B. Perimeter of the 27 December 2011 rock avalanche deposit, including the main
651 deposition area (yellow polygon) and the deposits lower-elevation deposits which have been
652 partially exposed to erosion by debris flows in 2012 (red polygon). The 2012 post-event digital
653 elevation model (lidar, blue polygon) is from 18 July 2012 (data courtesy of the Amt für Wald,
654 Canton Graubünden). Pre-event digital elevation model (lidar) for 2009 is from the SwissAlti3D
655 (version 2012) data set from swisstopo, ©2012, swisstopo (5704 000 000) . The grey solid arrow
656 indicates the main debris-flow channel formed in 2012.



657

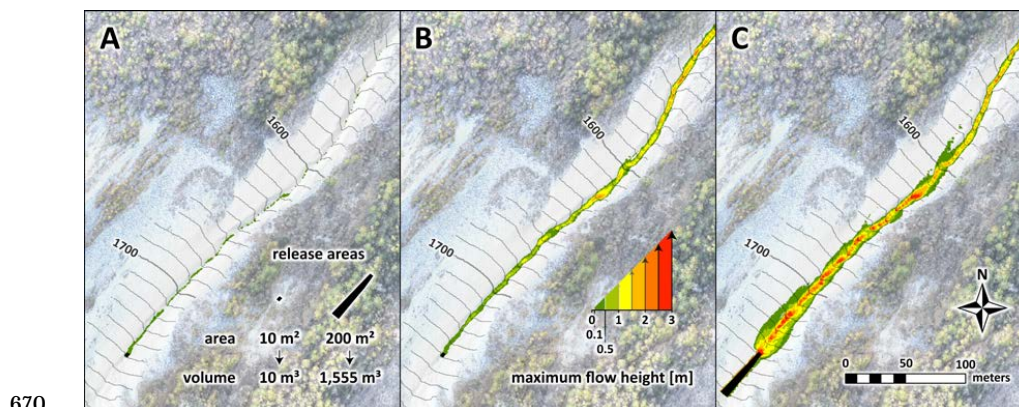
658 **Figure 3.** Calibration of modelled erosion patterns (**B1 to B3**) to the observed erosion depths (**A**) in
659 the upper open debris slopes of the “Bochtür” catchment (Meretschibach) by varying values for the
660 friction parameter μ . The blue polygon demarks the area where a differential DTM is available.



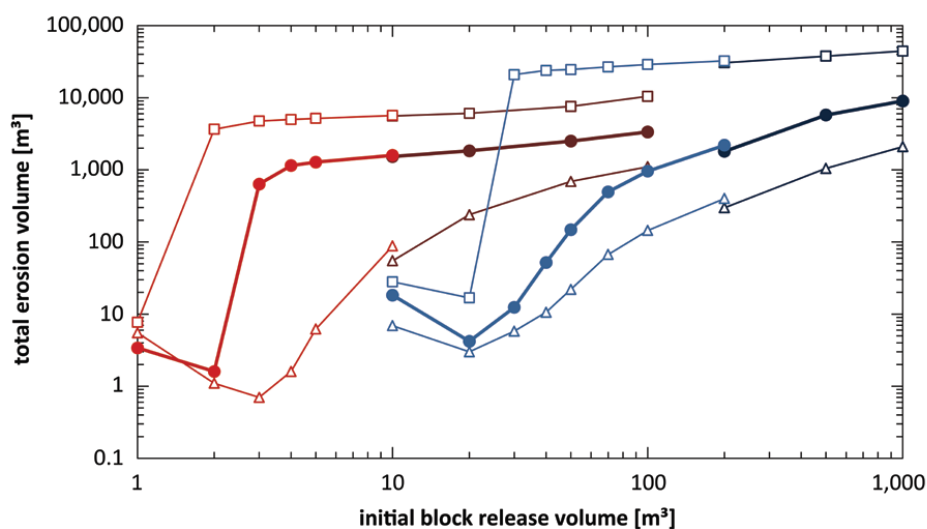


665

666 **Figure 5.** Overview of rock avalanche deposits, subsequently formed debris flow channels, and the
 667 resulting overall elevation change in the Bondasca catchment (A, B). The elevation change map
 668 2009 to 2012 (C) includes both the rock avalanche ($\approx 1.5 \text{ Mio m}^3$ on 27 Dec. 2011) and the first
 669 two debris flow events (5 and 14 July 2012).



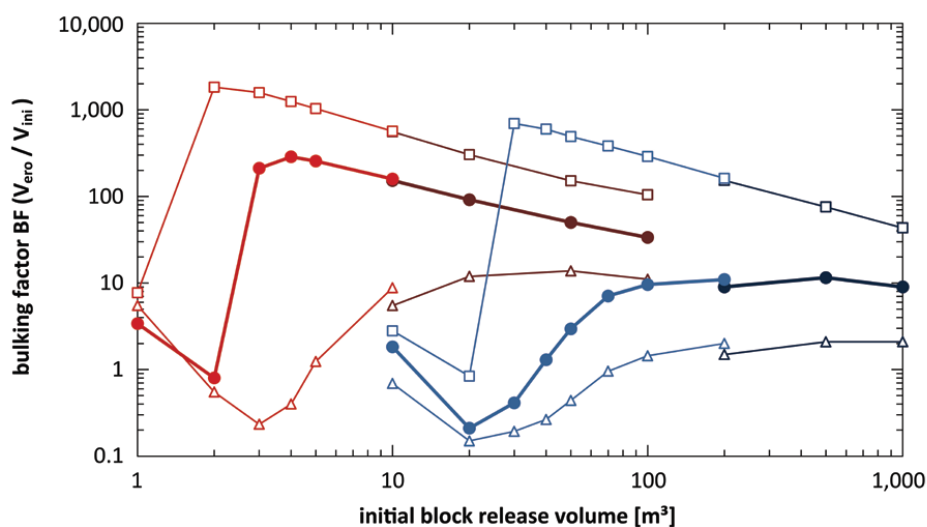
671 **Figure 6.** Comparison of runout patterns at “Bochtür” in the Meretschi catchment. The debris flow
672 modeling is conducted using a (subtract) block release volume of (A) 10 m³ and no-entrainment
673 modeling, of (B) 10 m³ and entrainment modeling as well as a total (subtract) block release volume
674 of (C) 1,555 m³ (sum of release and eroded volume from (B)) and no-entrainment modeling.



	Meretschi	Bondasca
calibrated parameters	$\xi = 200 \text{ m}^2\text{s}^{-1}, \mu = 0.60$	$\xi = 400 \text{ m}^2\text{s}^{-1}, \mu = 0.30$
release areas	— 10 m ² — 50 m ²	— 100 m ² — 500 m ²
erosion rates (Frank et al., 2015)	—△— 1.25 cm s ⁻¹ —●— 2.5 cm s ⁻¹	—□— 5.0 cm s ⁻¹

675

676 **Figure 7.** Sensitivity of modeled erosion volume to initial block release volume in the
 677 Meretschibach and in the Bondasca catchments.



	Meretschi	Bondasca
calibrated parameters	$\xi = 200 \text{ m}^2 \text{ s}^{-1}, \mu = 0.60$	$\xi = 400 \text{ m}^2 \text{ s}^{-1}, \mu = 0.30$
release areas	— 10 m ² — 50 m ²	— 100 m ² — 500 m ²
erosion rates (Frank et al., 2015)	—△— 1.25 cm s ⁻¹ —●— 2.5 cm s ⁻¹	—□— 5.0 cm s ⁻¹

678

679 **Figure 8.** The bulking factor $BF = V_{\text{ero}}/V_{\text{ini}}$ of the modeled total erosion volume $V_{\text{ero}} [\text{m}^3]$ to initial
 680 block release volume $V_{\text{ini}} [\text{m}^3]$ in the Meretschibach and Bondasca catchments.